View metadata, citation and similar papers at core.ac.uk
brought to you by CORE
provided by Wageningen University & Research Publications

Conformation of a Peptide Encompassing the Proton Translocation Channel of Vacuolar H^+-ATPase

Werner L. Vos, Louic S. Vermeer, and Marcus A. Hemminga
Laboratory of Biophysics, Wageningen University, Wageningen, The Netherlands

ABSTRACT The structural properties of a crucial transmembrane helix for proton translocation in vacuolar ATPase are studied using double site-directed spin-labeling combined with electron spin resonance (ESR) (or electron paramagnetic resonance) and circular dichroism spectroscopy in sodium dodecyl sulfate micelles. For this purpose, we use a synthetic peptide derived from transmembrane helix 7 of subunit *a* from the yeast *Saccharomyces cerevisiae* vacuolar proton-translocating ATPase that contains two natural cysteine residues suitable for spin-labeling. The interspin distance is calculated using a second-moment analysis of the methanethiosulfonate spin-label ESR spectra at 150 K. Molecular dynamics simulation is used to study the effect of the side-chain dynamics and backbone dynamics on the interspin distance. Based on the combined results from ESR, circular dichroism, and molecular dynamics simulation we conclude that the peptide forms a dynamic α-helix. We discuss this finding in the light of current models for proton translocation. A novel role for a buried charged residue (H729) is proposed.

INTRODUCTION

Vacuolar (H^+)-ATPase (V-ATPase) is a large multi-protein membrane-bound enzymatic complex present in almost all types of eukaryotic cells. The enzyme is an ATP-driven proton pump, acting as a molecular motor, which is responsible for the acidification of intracellular compartments in eukaryotic cells. Acidification of intracellular compartments or vacuoles is essential for various cellular processes, including ligand-receptor dissociation and protein processing and degradation (1,2). V-ATPases are also found in the cell membranes of specialized cells, where they function in processes such as renal acidification (3), pH homeostasis of macrophages (4), and bone resorption (5). Although structural information on the membrane-bound part of the protein is limited, this kind of information could be valuable in the search for new therapeutic agents to treat diseases that are related to bone resorption such as, for instance, osteoporosis. Moreover, structural studies of the membrane part of the protein could increase our insight into the complicated and yet poorly understood mechanism of protein translocation of V-ATPase.

V-ATPases have a membrane-bound domain, the V_O domain, and a water-soluble domain, the V_1 domain. ATP hydrolysis takes place at the V_1 domain, whereas protons are transported through the V_O domain. In yeast, the V_O domain comprises a hexameric ring, which is part of the rotary motor. It is composed of three different proteolipid subunits called *c* (Vma3p, 4×), *c′* (Vma11p, 1×), and *c″* (Vma16p, 1×). Each of the proteolipid subunits has a single buried glutamic acid that is essential for proton transport. The hexameric ring is in contact with subunit *a* (Vph1p or Stv1p), which plays the role of a stator in the molecular motor.

Subunit *a* is thought to provide access for protons to the buried sites of the proteolipid subunits via two hemichannels on the cytoplasmic and luminal side of the membrane. Subunit *a* is an integral membrane protein containing a cytoplasmic domain and a membrane-bound domain. The membrane-bound domain is thought to contain nine transmembrane helices (6) (for a complete topology model of subunit *a*, see Kawasaki-Nishi et al. (6)). The transmembrane (TM) helix 7 (TM7), which is the seventh putative transmembrane segment of subunit *a*, was proposed to comprise residues 727–752. It plays a pivotal role in proton transport, containing an essential arginine, R735, whose mutation completely inhibits proton translocation. Moreover it contains two buried histidine residues, H729 and H743, whose mutation affects proton transport, although these residues are not absolutely required for proton transport activity (7,8).

Here, we study a synthetic peptide derived from TM7 of subunit *a* from the yeast *Saccharomyces cerevisiae* V-ATPase (Fig. 1, *peptide I*) using circular dichroism (CD) and electron spin resonance (ESR) spectroscopy. Model peptides are suitable systems for spectroscopic and theoretical studies, since they give insight into local conformations and interactions that can be important in the native system (9–12). The amino acid sequence of this peptide is slightly shifted with respect to TM7, spanning residues 721–745 from subunit *a*, to span a small part of the loop region interconnecting TM7 and TM6 that comprises the putative binding site of the V-ATPase inhibitor bafilomycin (13). The structure of this segment in the intact protein is not completely clear. Most likely it is helical, extending from the membrane, as was suggested in the literature (13,14).

Although CD spectroscopy can provide valuable information on the secondary structure of a peptide or protein (15), it is not suitable for obtaining site-specific information. For this purpose, we employ ESR spectroscopy in combination with SDSL (site-directed spin-labeling). For doubly

Submitted May 23, 2006, and accepted for publication September 14, 2006.

Address reprint requests to Marcus A. Hemminga, Laboratory of Biophysics, Dreijenlaan 3, 6703 HA Wageningen, The Netherlands. Tel.: 31-317-482044; Fax: 31-317-482725; E-mail: marcus.hemminga@wur.nl.

© 2007 by the Biophysical Society

0006-3495/07/01/138/09 $2.00

doi: 10.1529/biophysj.106.089854

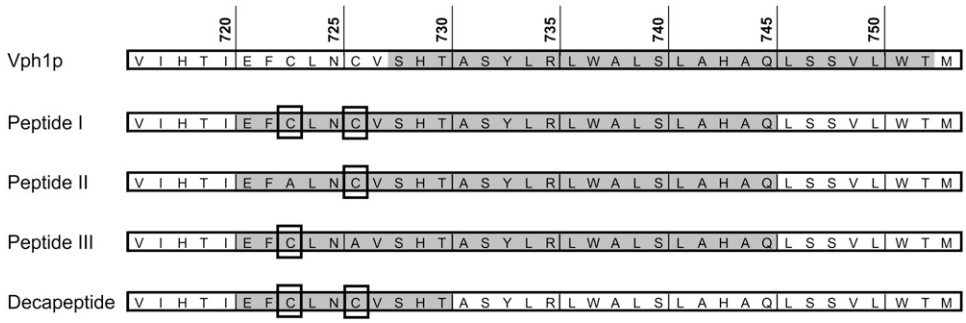

FIGURE 1 Putative transmembrane helix 7 (*TM7*, *gray shaded*) of subunit *a* of V-ATPase from the yeast *Saccharomyces cerevisiae* (2) and the peptides used in this work. The numbering of the amino acid residues corresponds to the numbering for the native subunit *a* (6). Peptide I (*gray-shaded sequence*) was used for CD and ESR experiments. The cysteine residues that were spin-labeled are indicated by square windows. Peptides II and III are Cys-Ala mutants of peptide I that were used as references for the ESR second-moment analysis. The decapeptide is a truncated version of MTSSL-labeled peptide I, which was used exclusively for the MD simulations.

spin-labeled proteins, ESR spectroscopy has proven to be useful as a spectroscopic ruler (16), in particular for structural studies of membrane proteins (17). The primary sequence of peptide I contains two native cysteine residues, C723 and C726, that were specifically labeled with ESR spin probes. Using ESR spectroscopy as a spectroscopic ruler, site-specific structural information can be obtained on doubly spin-labeled peptide I. Here, we calculate the interspin distance between spin-labeled residues C723 and C726 using a second-moment spectral analysis.

The interspin distance is interpreted using molecular dynamics (MD) simulations. To save computer time, a truncated version of the original peptide containing the cysteine residues was used for the MD simulations (Fig. 1). The sequence overlaps partly with the loop region interconnecting TM6 and TM7, and partly with TM7. In the intact protein, TM7 is adjacent to TM8 of subunit *a*, and to TM4 of subunit *c*′. Hence, in the intact protein, the direct environment of the studied residues most likely is a combination of other TM helices, water, and phospholipids. Recently, it was shown that the structural features of a membrane peptide were similar in water and in a lipid membrane (18), suggesting that its conformation is mainly determined by its amino acid sequence rather than by its direct environment. For this reason, we use pure water as a solvent in our MD simulations. The combined data from CD spectroscopy, ESR spectroscopy, and MD simulations show that the cytoplasmic part of the isolated TM7 forms a dynamical α-helix when bound to sodium dodecyl sulfate (SDS) micelles. This finding is discussed in view of the current model for proton translocation that assumes swiveling of the helices in subunits *a* and *c* upon proton translocation (19).

METHODOLOGY

Peptide design and synthesis

Based on the primary sequence of TM7 from subunit *a* from yeast (2), a 25-residue peptide was designed (Fig. 1, *peptide I*). The peptide was designed to include the essential arginine R735, which was shown to be absolutely required for proton translocation, as well as the two nearby histidines H729 and H743. In addition, the peptide was selected to contain two cysteines, C723 and C725, which are part of the proposed cytoplasmic hemichannel and loop between TM6 and TM7. These cysteines are suitable targets for SDSL. A combination of these prerequisites resulted in peptide I, spanning the amino acid residues 721–745 of subunit *a*. Throughout this article, the numbering of the amino acid residues in peptide I will be the same as that used for the native subunit *a* (Fig. 1). To enable single cysteine mutants for SDSL, two additional peptides, II and III, were designed in which cysteines C723 and C725 were replaced by alanines (Fig. 1). All peptides were produced by Pepceuticals Ltd (Leicester, UK) on solid support using continuous-flow chemistry. Peptides were >90% pure, as determined by high-performance liquid chromatography and mass spectrometry.

Spin-labeling

For spin-labeling, typically an amount of 2.5 mg of peptides I–III was dissolved in 750 μl dimethylsulfoxide and 250 μl water in a plastic tube. Subsequently, 100 μl 9.5 mM methanethiosulfonate spin label (MTSSL (1-oxy-2,2,5,5-tetramethyl-Δ^3-pyrroline-3-methyl)methanethiosulfonate)) stock in dimethylsulfoxide was added and the tube was slowly vortexed for 3 h at room temperature. MTSSL was purchased from Toronto Research Chemical (Toronto, Ontario, Canada). Small amounts of sample (10 μl) were stored at -18°C for matrix-assisted laser-desorption/ionization time-of-flight (MALDI-ToF) measurements; the remaining part of the sample was immediately purified on a superdex-75 gel column using 10 mM SDS as eluent, buffered at pH 7.0 with 10 mM Na_2HPO_4. The flow speed was 60 ml/min, and every 2 min, a fraction was collected. Fractions containing the spin-labeled peptides were detected by monitoring the fluorescence at 350 nm with a Fluor LC 304 by LINEAR, using an excitation wavelength of 280 nm. Only the fraction with the highest fluorescence intensity was used for further experiments, typically appearing after ~52 min.

CD measurements

Peptide samples for CD spectroscopy were made up in 50 mM SDS and buffered at pH 7.0 by Na_2HPO_4. The final peptide concentrations were 47 and 52 μM for labeled and unlabeled peptide I, respectively. Far-UV CD spectra were recorded at 20°C on a Jasco J-715 CD spectropolarimeter in a 0.1-mm quartz cuvette and corrected for the SDS background. The cuvette house was flushed with a constant stream of nitrogen to remove oxygen that could interfere with the CD measurements. The observed CD signal was converted to the mean residue ellipticity ($[\theta]$ in deg cm^2 dmol^{-1}) as follows (11):

$$[\theta] = \theta/10lcn. \quad (1)$$

Here, θ is the CD signal in mdeg, l is the optical path length in cm, c is the concentration of peptide in molars, and n is the number of amino acid residues in the peptide.

Peptide concentrations were determined based on the absorbance at 280 nm after correcting for the SDS background via the extinction coefficients of tryptophan, tyrosine, and the nitroxide spin label. For the calculation of the extinction coefficients, the effects of tryptophan oxidation and incomplete spin-labeling were taken into account as described elsewhere (20). UV absorption spectra were recorded in a 1-mm quartz cuvette with a Varian (San Carlos, CA) Cary 5E at room temperature.

The percentage of α-helix content $\{\alpha\}$ of the labeled and unlabeled peptide I was estimated by assuming that the ellipticity at 222 nm is exclusively due to α-helix conformation (11,21):

$$\{\alpha\} = \frac{[\theta]_{222}}{[\theta]_{222}^{\max}}\left(1 - \left(\frac{k}{n}\right)\right)\times 100, \quad (2)$$

where $[\theta]_{222}$ and $[\theta]_{222}^{\max}$ are the experimental and maximal ($-39{,}500$ deg cm^2.dmol^{-1}) values, respectively, of the ellipticity at 222 nm. The wavelength dependent constant k is 2.57 at 222 nm.

ESR measurements

ESR spectra were recorded on an X-band ELEXSYS E500 (Bruker, Berlin, Germany) equipped with a super high-sensitivity probehead in combination with a SuperX bridge. Temperature was kept at 150 K with a quartz variable temperature Dewar insert. Spectra were recorded at 20 mT scan widths with a low microwave power (0.2 mW) to avoid saturation. The ESR spectrum of doubly spin-labeled peptide I was corrected for singly labeled, noninteracting species based on the MALDI-ToF spectra of peptides II and III. Because the ESR spectra of spin-labeled peptides II and III were identical, the ESR spectrum of spin-labeled peptide III was not used in this correction. Details of the MALDI-ToF work and the correction procedure are described in a separate article (20).

The distance between two spin labels depends on the second moments of the ESR spectra via (22,23)

$$r = 2.32/(\Delta M_2)^{1/6}. \quad (3)$$

Here, r is the distance between the paramagnetic centers in nanometers, and ΔM_2 is the difference in spectral moment between the doubly (M_D) and singly (M_S) labeled spectra in units $10^{-8}\,T^2$:

$$\Delta M_2 = M_D - M_S, \quad (4)$$

with

$$M_D = \frac{\int (B - B_{FD})^2 G_D(B) dB}{\int G_D(B) dB} \quad (5)$$

and

$$M_S = \frac{\int (B - B_{FS})^2 G_S(B) dB}{\int G_S(B) dB}. \quad (6)$$

Here, $G_D(B)$ is the absorption spectrum of the doubly spin-labeled protein sample and $G_S(B)$ is the corresponding spectrum without dipolar interaction. M_D and M_S are obtained by numeric integration of the first derivative absorption spectrum. B_{FD} and B_{FS} are the first spectral moments of doubly- and singly labeled peptide, respectively, and B is the magnetic field.

Molecular dynamics simulations

To limit the amount of computational time, a truncated version of peptide I was used for the MD simulations. This artificial decapeptide comprises amino acid residues 721–730 (Fig. 1) and includes cysteine residues C723 and C726, which were used in the spin-labeling work. Although high-resolution data of subunit a are not available at this moment, it has been suggested that residues 721–727 are α-helical, extending toward the cytoplasm (13,14). Residues 728–730 are also expected to be α-helical, since they are part of TM7 (6). Therefore the backbone dihedral angles of the starting conformation of the decapeptide were set to the values of an ideal α-helix, being $\phi = -62°$ and $\psi = -41°$ (24). To investigate the effect of biasing toward an α-helical starting conformation, a second simulation was performed with a 3_{10}-helical starting conformation, using dihedral angles of $\phi = -49°$ and $\psi = -26°$. In both simulations, the dihedral angles of the side chains were initially set to an all-*trans* configuration.

MD simulations were performed with the GROMACS software package (25,26), using the GROMOS96 force field (27). The force field of the spin-labeled cysteine residue was made based on the building blocks of cysteine and TEMPO that are part of the standard GROMOS96 force field, and can be obtained from the authors on request. For the natural protein, residues 721–730 of subunit a are located in or close to the cytoplasm (2). For this reason, the artificial decapeptide was solvated in explicit single-point-charge water, using a total of ~2000 water molecules. A triclinic box was used with box dimensions $a = b = c = 4.0$ nm; the net charge was 0. The energy of the system was minimized using a steepest-descent algorithm. The final coordinates from the minimization were used for two 20-ns production runs. During the first part of the simulations (0–10 ns), a restraining potential of 1000 kJ mol^{-1} nm^{-2} was applied on the C_α atoms to keep the peptide in an α- or 3_{10}-helical conformation. This restraining potential was released during the second part (10–20 ns) of the production run. The MD simulations were carried out using periodic boundary conditions. The temperature was controlled by coupling separately the peptide and the water to a temperature bath at 325 K using a Berendsen thermostat (28). A constant pressure of 1 bar was applied independently in all three directions using a coupling constant of 0.5 ps. Nonbonded interactions were treated with a twin-range cutoff scheme. Within a short-range cutoff radius of 0.8 nm, the interactions were evaluated at every time step based on a pair list that was updated every five steps. Intermediate-range interactions up to a long-range cutoff of 1.4 nm were evaluated with every pair list update and assumed constant in between. To account for electrostatic interactions beyond the long-range cutoff radius, a reaction-field approximation was applied (29,30) using a relative dielectric permittivity of 54 for the solvent.

RESULTS

Circular dichroism

The CD spectrum of MTSSL-labeled peptide I in SDS micelles (Fig. 2) has two minima at 208 and 222 nm, indicative for an α-helix. Using Eq. 2, the α-helix content $\{\alpha\}$ was calculated to be 32 ± 3%. The unlabeled peptide I has minima at slightly different wavelengths: 209 and 224 nm, also suggesting an α-helical conformation. For this peptide, the calculated α-helix content is 33 ± 3%.

For an ideal α-helix, the value of the ratio of the peak intensities at 208 and 222 nm, $[\theta]_{222}/[\theta]_{208}$, typically is 0.83 (31). A value >1 is an indication for the formation of coiled coils (11,32). The CD spectrum of labeled peptide I gives a ratio of 0.88, which is close to the value of an ideal α-helix. For the unlabeled peptide I, this ratio is 1.05, suggesting the formation of coiled coils.

ESR spectroscopy

For rapidly tumbling peptides, the dipole-dipole interaction tensor between the two spin labels averages to zero and does not contribute to the ESR spectrum. Therefore, the ESR

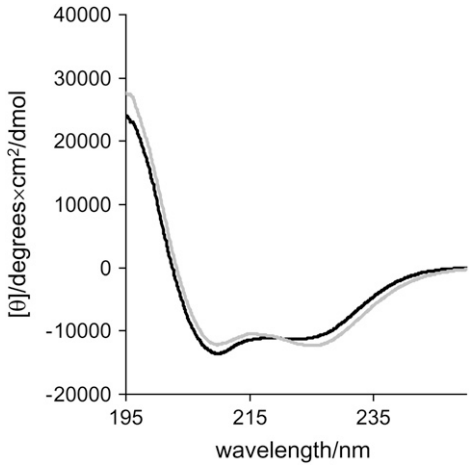

FIGURE 2 CD spectra of the spin-labeled (*black*) and unlabeled peptide I (*gray*) in 50 mM SDS micelles, buffered at pH 7.0 by Na_2HPO_4. The spin label used is MTSSL. Peptide concentrations were 47 and 52 μM for labeled and unlabeled peptide I, respectively. Spectra were recorded at 20°C.

spectra were recorded at 150 K, where motional averaging effects are not present (33). The ESR spectra of singly labeled peptide II and doubly labeled peptide I in frozen solution at 150 K are presented in Fig. 3, *A* and *B*, respectively.

The ESR spectrum of singly labeled peptide II (Fig. 3 *A*), in which there are no interacting spin labels, has the characteristic shape of a powder spectrum, indicating that the spin labels are immobilized on the ESR timescale. The ESR spectrum of doubly labeled peptide I (Fig. 3 *B*) is clearly broadened with respect to the singly labeled peptide II due to dipolar interaction. Consequently, the second moment of the doubly labeled peptide is larger than the second moment of the singly labeled species (see Table 1). From Eq. 3, the interspin distance was calculated from the difference in second moments to be $r = 0.94 \pm 0.06$ nm.

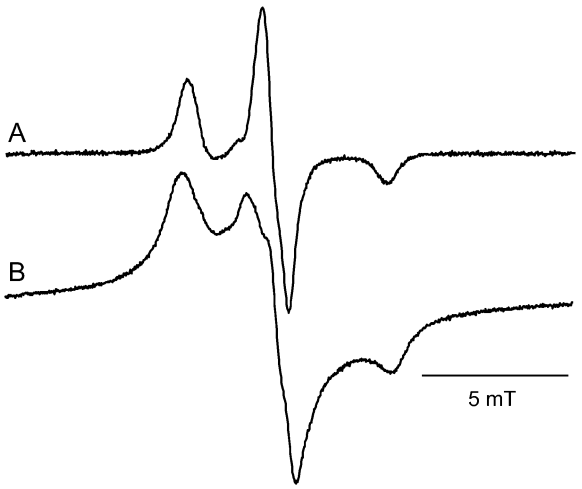

FIGURE 3 ESR spectra of the singly labeled peptide II (A) and doubly labeled peptide I (B) in 50 mM SDS, buffered at pH 7.0 by Na_2HPO_4. The spin label used is MTSSL. Peptide concentrations were 16 and 47 μM for peptides II and I, respectively. The spectrum of doubly labeled peptide I was corrected for the contribution of noninteracting spin labels based on MALDI-ToF mass spectrometry using the spectrum of peptide II (20). The temperature is 150 K.

For the interpretation of the ESR results it is crucial that the dipolar broadening in doubly spin-labeled peptide I arises from intra and not from intermolecular interactions. To check whether aggregates were formed due to noncovalent protein-protein interactions, the peptide sample was titrated with a concentrated SDS stock solution of 0.3 M, buffered at pH 7.0. SDS is known as a strong detergent that has the ability to disrupt noncovalent protein-protein interactions; hence, an excess of SDS is expected to disrupt peptide aggregates when present (34). For SDS/peptide ratios of 1:900 and 1:1600 the interspin distances were identical within the experimental error, showing that the peptides were essentially monomeric. This strongly indicates that the dipolar interaction is intramolecular.

DISCUSSION

Circular dichroism spectroscopy

The CD spectra of labeled and unlabeled peptide I are almost similar in terms of intensity and shape, indicating that overall their conformations are approximately the same. The intensity in the spectra is strongly reduced as compared to an ideal α-helix, leading to an α-helix content of ~32%. We ascribe this reduction in CD signal and the corresponding low α-helix content to dynamics of the peptide backbone. Small α-helical peptides are expected to behave as fluctuating semibroken rods (35). From theoretical studies, it is known that smaller helices give a lower mean residue ellipticity (36). Therefore, breaking up an α-helix into smaller α-helical segments will lead to a CD signal with a reduced intensity. Thus, the CD results could indicate that peptide I is a flexible α-helix undergoing rapid changes between multiple conformational states.

X-ray studies of spin-labeled proteins have demonstrated that MTSSL is generally well tolerated in α-helical structures (37,38). Also in our study, the CD spectra of labeled and unlabeled peptides are similar, indicating that the structure is not affected by the presence of the spin labels. Nevertheless, a small difference is seen in the ratio $[\theta]_{222}/[\theta]_{208}$. For labeled peptide I, the value of $[\theta]_{222}/[\theta]_{208}$ is well below 1, indicating monomeric α-helices. For the unlabeled peptide I, $[\theta]_{222}/[\theta]_{208}$ is 1.05, suggesting the formation of a coiled-coil structure. Previously, it has been shown that a single cysteine residue can promote the formation of coiled coils via the formation of disulfide bridges (39,40). Our peptide has two

TABLE 1 Parameters for the interspin distance calculation using the second-moment analysis of the ESR spectra in Fig. 3

$M_S/10^{-8}$ T^2	$M_D/10^{-8}$ T^2	$\Delta M_2/10^{-8}$ T^2	r/nm
390 ± 5*	622 ± 5*	232 ± 7	0.94 ± 0.06

*Error limit taken from Wegener et al. (55).

native cysteine residues that enable the formation of cysteine cross-links, probably promoting the formation of coiled-coil structures. When the spin labels chemically block the cysteine residues, there is no indication for coil-coil formation. This suggests that the presence of the chemically reactive cysteine residues is the determining factor for the formation of a coiled coil. Therefore we interpret the formation of coiled coils in the case of unlabeled peptide I as an artifact related to the chemical properties of the peptide rather than an intrinsic property of the amino acid sequence.

ESR spectroscopy

For a perfect α-helix, the interspin distance of 0.94 nm can be related to the structure of the peptide via a simple calculation. In a simplified model, the spin labels are regarded as a rigid stick. This stick is defined as the line perpendicular to the helix axis intersecting the cysteine C_β-atom. For MTSSL, the length of the stick was estimated to be 0.7 nm (16). We define the interspin distance as the distance between the ends of the two sticks. In our case, with the spin label attached to cysteine residues C723 and C726, the interspin distance is calculated to be 0.80 nm. This simple calculation already shows that the peptide does not form an ideal α-helix.

A similar calculation was carried out for a perfect 3_{10}-helix. These helices are frequently found in small membrane peptides (41), because in a 3_{10}-helix the free-energy loss associated with unsatisfied hydrogen bonds at the termini is smaller than in an α-helix (42). In the case of a 3_{10}-helix, the calculated interspin distance is 0.60 nm (see Table 2), which is even less in agreement with the experimental value. The observation that the distances are smaller than the distance calculated from the second-moment analysis can be explained by dynamics of the spin-labeled side chains, or by the fact that the backbone of the peptide is flexible, resulting in a nonperfect helical conformation.

To test these ideas, the effect of side-chain dynamics on the interspin distance was investigated by performing MD simulations that explicitly take into account the force field and molecular structure of MTSSL. To reduce the computer time, we constructed an artificial decapeptide, which is a truncated version of the original peptide containing cysteine residues C723 and C726 (Fig. 1). In the intact protein, lateral forces arising from the connecting loop region between TM6 and TM7 could cause forced bending of the amino acid sequence studied here, prohibiting the formation of an α-helical structure in the loop. However, since the loop is sufficiently long to accommodate lateral forces (74 amino acid residues, as compared to ~10 residues for a typical loop region), we assume that a forced bending of the loop region does not affect the structure of the amino acid sequence. In the first part of the MD simulation (0–10 ns), the backbone of the decapeptide was kept in a fixed 3_{10} or α-helix conformation by putting a restraining potential on the C_α atoms. For an α-helical starting conformation, the MD result is shown in Fig. 4. The number of amino acid residues in an α-helical conformation is six to seven, close to the maximal value of eight. Note that the ''define secondary structure of proteins'' (DSSP) algorithm (43) that is used to calculate the α-helical residues does not count the terminal residues of the decapeptide, since no sufficient hydrogen bonds can be formed with adjacent residues in the termini. Occasionally, a few residues are in a 3_{10}-helix conformation. Initially (0–2 ns), the interspin distance fluctuates rapidly with values between 0.5 and 1.2 nm. These fluctuations probably arise from the rather arbitrary (all-trans) configuration of the side chains. After 2 ns, the interspin distance fluctuates mostly between 0.5 and 0.9 nm.

To minimize effects of the starting conformation, the time-averaged interspin distance was calculated for the last 5 ns (5–10 ns) (see Table 2). The value of 0.79 nm is in excellent agreement with the value calculated for the simple helical model (0.80 nm), indicating that dynamics of the peptide backbone and the related distortion of the backbone conformation are responsible for the increase in interspin distance. The distance distribution over the last 5 ns of MD simulation (5–10 ns) is shown in Fig. 5. A strong peak is found at a distance of 0.90 nm, and a smaller one at 0.65, arising from different rotameric states of the spin label. This indicates that multiple rotameric states are accessible, despite the fact that the backbone is kept in a fixed α-helix.

The same approach was taken to calculate the interspin distance for a 3_{10}-helical starting conformation, also time-averaging the interspin distance over the last 5 ns of MD simulation (see Table 2). The averaged interspin distance of 0.65 nm is also close to the value calculated for the simple model (0.60 nm). This could indicate that for α- and 3_{10}-helices with a rigid backbone, a simple stick model is sufficient to calculate the interspin distance. Since the calculated average distances for both an α-helix and a 3_{10}-helix are close to the distances calculated with the simple helical models, and since the distances are smaller than the value that was calculated with the second-moment analysis, we conclude that the peptide does not form a rigid α- or 3_{10}-helix. Possibly, dynamics of the peptide backbone and the related distortion of the backbone conformation are responsible for the increase in interspin distance.

To test the effect of flexibility of the backbone on the interspin distance, the restraining potential was removed

TABLE 2 Interspin distances calculated for a simple helix model and for MD trajectories of spin-labeled artificial decapeptide starting from α- and 3_{10}-helix conformations

		Average interspin distance (nm)	
Model type	Time interval (ns)	3_{10}-Helix starting conformation	α-Helix starting conformation
Simple helix	NA	0.60	0.80
Restrained backbone	5–10	0.65	0.79
Free backbone	15–20	0.83	0.89

Decapeptides are Peptides I–III, as described in Fig. 1. NA, not applicable.

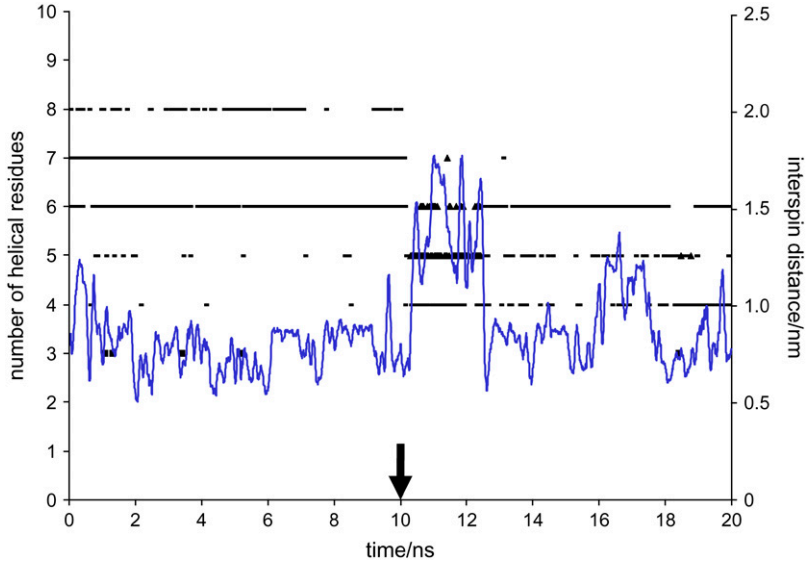

FIGURE 4 Number of helical residues in terms of 3_{10}-helix (■), α-helix (*dashed lines*), and π-helix (▲) (*left axis*) and interspin distance (*right axis*) in the MD simulation of the MTSSL-labeled artificial decapeptide starting from an α-helix conformation. The interspin distance is defined as the distance between the centers of mass of the nitroxide groups. During the first half of the simulation (0–10 ns), a restraining potential on the C_α atoms was used to keep the peptide in an α-helix conformation. The arrow indicates the time (10 ns) at which the restraining potential was removed. Snapshots were taken every 10 ps. Helix types were assigned according to the DSSP algorithm (43). Note that this algorithm does not count the terminal amino acid residues. Because of crowding of the data points on the horizontal axis, they are not shown (most of the time, the number of residues in the 3_{10}- or π-helix is zero).

after the first 10 ns of the MD simulations (Fig. 4, *black arrow*). As can be seen for an α-helical starting conformation, this results in a reduction of the number of residues in an α-helical conformation to four to six. In the first 3 ns after releasing the backbone constraints (10–13 ns), about half of all amino acid residues are in a π-helix conformation. The π-helix never persists longer than 90 ps, indicating that the π-helix is not very stable. The presence of a metastable π-helix conformation is interesting. Although a clear role of the π-helix has not been established in protein structure and function (44,45), it has been suggested that the π-helix is a metastable helix that marks systems with a high propensity for conformational transitions (46). We therefore regard the π-helix as a metastable structure indicating a conformational flexibility of the peptide. Nevertheless, the π-helix may still be an artifact of simulations on small peptides. In the GROMOS96 force field, it is actually favored over the α-helix by -0.3 kcal/mol (47). Therefore, it could be that the amount of π-helix in the MD simulations is overestimated. Throughout the last part of the simulation (12.5–20 ns), the α-helix is the dominant structure. The formation of the π-helix is accompanied by a sudden increase in interspin distance, fluctuating between 1.2 and 1.8 nm. Once the α-helix is formed, the interspin distance decreases to <1.0 nm, with another increase between 16 and 17.5 ns. However, this second increase in interspin distance is not accompanied by the formation of a π-helix.

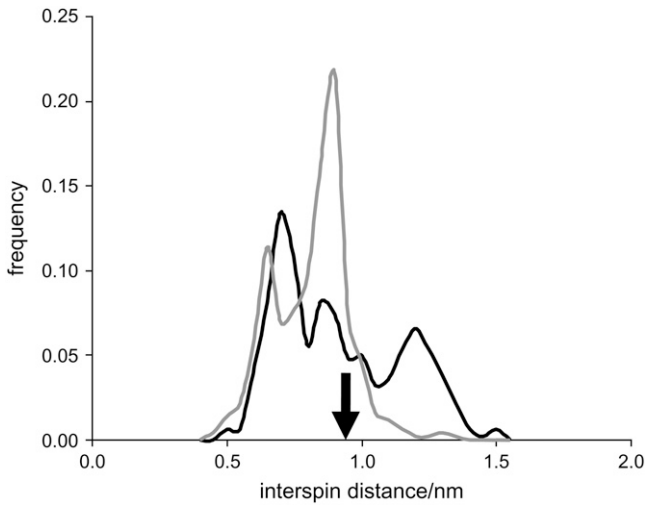

FIGURE 5 Interspin distance distributions from the MD trajectory of the MTSSL-labeled artificial decapeptide starting from an α-helix conformation. (*Gray line*) Distances taken from the 5–10 ns part of the simulation in the presence of a restraining potential on the C_α atoms to keep the peptide in an α-helix conformation. (*Black line*) Distances taken from the 15–20 ns part of the simulation after release of the restraining potential at 10 ns. Interspin distances were taken from 10-ps snapshots. The arrow indicates the interspin distance calculated from the second-moment analysis (0.94 nm). The area of the distributions is normalized to 1.

To minimize the effect of the starting structure, the average interspin distance was calculated for the last part of the simulation (15–20 ns). In this part of the simulation, the time-averaged interspin distance is 0.89 nm, which is in good agreement with the value of 0.94 ± 0.06 nm calculated from the second-moment analysis. As compared to the restrained part of the MD simulation, the distance distribution broadens and peaks appear at 0.70, 0.85, 1.00, and 1.20 nm, probably arising from an increase in rotameric states of the spin label. Therefore, the increase of the average interspin distance can be explained by flexibility of the peptide backbone, even though the peptide remains α-helical most of the time. For a 3_{10}-helical starting conformation, a similar MD simulation results in an average distance of 0.83 nm (see Table 2). Although this average distance is smaller than in the case of an α-helical starting conformation (0.89 nm), the average distance is strongly increased with respect to the fixed 3_{10}-helix (0.65 nm). Also, this interspin distance is larger than in the case of a fixed α-helix (0.79 nm). This could suggest that

both simulations converge to a similar structure, independent of the starting conformation used. Relaxation dynamics of secondary structure can occur on much larger timescales than the timescales used in our work (48), which might explain the small difference between the average interspin distance calculated for a flexible α-helix and a flexible 3_{10}-helix.

Despite the fact that the interspin distance calculated from second-moment analysis represents a spatial average over a frozen distribution of conformations at 150 K, and the interspin distances from the MD simulations represents a time-average in the nanosecond range at 325 K, the good correspondence between the two averages is striking. Based on this result, we conclude that the peptide forms a flexible α-helix when bound to SDS micelles.

To illustrate the location of the α-helical residues in the second part of the simulations, the percentage of α-helix conformation per residue is plotted for both an α-helical and a 3_{10}-helical starting conformation in Fig. 6 (*black bars* and *red bars*, respectively). To limit biasing of the results toward the starting conformation, the percentage of α-helix per residue was averaged over the last 5 ns of the simulation (15–20 ns). Note, again, that the DSSP algorithm does not count the terminal amino acid residues E721 and T730. From this plot, it can be seen that residues F722–V727 form a relatively stable α-helical core around cysteine residues C723 and C726. Residues S728 and H729 do not show a significant percentage of α-helix, suggesting a more flexible conformation in the C-terminal domain of the decamer.

In the case of a 3_{10}-helical starting conformation, it is observed that the 3_{10}-helix converts rapidly into an α-helix. In fact, the percentage of 3_{10}-helix is negligible over the unrestrained part of the simulation (10–20 ns, data not shown). However, the percentage of α-helix per residue is slightly lower in the case of a 3_{10}-helical starting conformation compared to the simulation with an α-helical starting conformation. This small difference can be explained by the fact that the simulation time may be too short to ensure complete convergence. Taking all MD results together, we conclude that the amino acid sequence from F722 to V727 has a strong intrinsic tendency to form an α-helix. In comparison, S728 and H729 are relatively flexible.

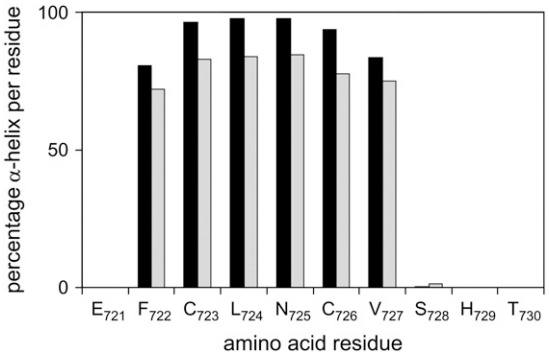

FIGURE 6 The percentage of α-helix per residue of the amino acid residues calculated from the MD trajectories of the MTSSL-labeled artificial decapeptide starting from an α-helical conformation (*black bars*) and from a 3_{10}-helical conformation (*gray bars*). The percentage of α-helix was calculated according to the DSSP algorithm (43). Note that this algorithm does not count the terminal amino acid residues. To limit biasing of the results toward the starting conformation, the percentage of α-helix per residue was an average over the last 5 ns of the simulation (15–20 ns).

In this work, we have employed a combined approach of CD spectroscopy, ESR spectroscopy, molecular modeling, and MD simulations to study the characteristics of a peptide I that is derived from an essential part of the proton translocation domain of V-ATPase. The results from CD spectroscopy show that the presence of the spin label does not have a pronounced effect on the conformation of the peptide. In addition, the CD results suggest that peptide I is flexible α-helix. The ESR results clearly indicate that the peptide is not a rigid α-helix, since the interspin distance is increased compared to that of a rigid α-helix. By using MD simulations we show that this increased interspin distance cannot be explained solely by side-chain dynamics, but results from backbone flexibility.

The amino acid sequence of peptide I (V721–Q745) overlaps with the putative α-helical TM7 of V-ATPase subunit *a* (6), which was predicted to comprise amino acid residues V727–T752. Residues E721–C726 of peptide I overlap with the putative cytoplasmic loop between TM6 and TM7. There is evidence from the literature that these amino acid residues are also in an α-helical conformation (13,14). Our spectroscopic results and MD simulations converge to support the view that peptide I is in an α-helical, albeit flexible, structure, suggesting that the amino acid sequence has a strong intrinsic propensity to adopt an α-helical conformation.

The increased flexibility of the C-terminus of the decapeptide with respect to the N-terminus is interesting. Previously it was shown in both experimental (49) and theoretical (50) work that in an α-helix, the two termini are not equivalent. In general, the backbone carbonyl groups of the last three residues of an α-helix are not hydrogen-bonded. Therefore, the backbone entropy of the C-terminus is larger than in the N-terminus, making the C-terminus more flexible than the N-terminus. Most likely, the increased flexibility of residues S728 and H729 reflects this phenomenon.

In addition, the backbone displays another type of flexibility, possibly due to thermal motions of the peptide backbone. Because of this, the number of rotameric states that are accessible increases, giving an overall increase in the interspin distance. Therefore, the combined results from the ESR experiment and the MD simulations could be explained by assuming that the peptide forms an α-helix, and that the increase in interspin distance arises from thermal fluctuations.

However, the calculated α-helix content of stable isolated transmembrane peptides bound to SDS micelles typically ranges from 60% to 80% (11), whereas our CD results give a calculated α-helix content of 33%. Moreover, the presence of a metastable π-helix indicates that the system has a high propensity for conformational transitions (46). We ascribe the low percentage of α-helix and the presence of a π-helix by

assuming that the α-helix breaks up into smaller fragments on the ns timescale, analogous to the model presented in the literature that assumes that α-helical peptides behave as fluctuating semibroken rods (35) that can twist and reorient independently of each other. Such breaking up of the α-helix would explain the lower CD signal, since smaller α-helices give a lower CD signal (36). This model is in good agreement with our finding of a π-helix, since the presence of a π-helix indicates that the region containing the cysteine residues has a high propensity to undergo conformational transitions, such as, for instance, breaking up of the helix into smaller fragments.

Proton translocation in V-ATPase subunit *a* is thought to occur through a rotary mechanism, in which arginine R735 in TM7 is brought into close proximity to the specific glutamic acid residues in the subunit *c* assembly, facilitating proton release (51). Cysteine cross-linking studies have indicated that TM7 of subunit *a* and TM4 of subunit c' are in close proximity in the V-ATPase, but the results were not consistent with a unique orientation of these two helical segments with respect to each other. Because of the diversity of the sites that could be cross-linked between TM7 and TM4, it was suggested that one or both of these helices could rotate with respect to each other (52). In this light, our finding of an α-helix breaking up into smaller fragments is interesting, since the helix swiveling that was found in the literature could be equivalent to the twisting of smaller fragments with respect to each other in our peptide model. For instance, breaking or loosening of the helix at the position of the cysteine residues would enable twisting of the TM-section with respect to the section toward the cytoplasm, moving independently of the cytoplasmic loop region.

We speculate that twisting or swiveling of TM7 is important for the gating of the cytoplasmic proton hemichannel, similar to the gating mechanism in other pore-lining helices of other ion channels, such as the nicotinic acetylcholine receptor (53). Interestingly, also in the case of the ErbB-2 tyrosine kinase receptor, a $\alpha \rightarrow \pi$-helix transition was found, causing a rotation of 100° about the helix axis, inducing changes in the distribution of the residues along the helix faces (54). For comparison, TM7 is thought to undergo a rotation of 60°–90° during proton transport (51). The swiveling could thus be important for the positioning of residues that are involved in channel gating, possibly H729, whose mutation has been shown to affect protein activity (6). At the same time, swiveling of the helix could be important for the positioning of the essential R735, allowing interaction with the glutamic acid residue of either subunit c' or c'', facilitating release of the proton into the luminal hemichannel. The V-ATPase inhibitor bafilomycin was shown to interact with residues E721, L724, and N725 (13). Based on our concept, inhibitor binding could rigidify the helix, thereby hampering or blocking proton translocation.

We thank Dr. Heinz-Jürgen Steinhoff (Experimental Physics, Macromolecular Structure, Universität Osnabrück) for providing the software to do the second-moment analysis. We thank the members of the MIVase consortium. We acknowledge Dr. Igor V. Borovykh for help with the ESR measurements.

This work was supported by contract No. QLG-CT-2000-01801 of the European Commission (MIVase—New therapeutic approaches to osteoporosis: targeting the osteoclast V-ATPase).

REFERENCES

1. Finbow, M. E., and M. A. Harrison. 1997. The vacuolar H^+-ATPase: a universal proton pump of eukaryotes. *Biochem. J.* 324:697–712.
2. Nishi, T., and M. Forgac. 2002. The vacuolar (H^+)-ATPases: nature's most versatile proton pumps. *Nat. Rev. Mol. Cell Biol.* 3:94–103.
3. Brown, D., S. Gluck, and J. Hartwig. 1987. Structure of the novel membrane-coating material in proton-secreting epithelial cells and identification as an H^+-ATPase. *J. Cell Biol.* 105:1637–1648.
4. Swallow, C. J., S. Grinstein, and O. D. Rotstein. 1990. A vacuolar type H^+-ATPase regulates cytoplasmic pH in murine macrophages. *J. Biol. Chem.* 265:7645–7654.
5. Chatterjee, D., M. Chakraborty, M. Leit, L. Neff, S. Jamsa-Kellokumpu, R. Fuchs, and R. Baron. 1992. Sensitivity to vanadate and isoforms of subunits A and B distinguish the osteoclast proton pump from other vacuolar H^+-ATPases. *Proc. Natl. Acad. Sci. USA.* 89:6257–6261.
6. Kawasaki-Nishi, S., T. Nishi, and M. Forgac. 2003. Proton translocation driven by ATP hydrolysis in V-ATPases. *FEBS Lett.* 545:76–85.
7. Leng, X.-H., M. F. Manolson, and M. Forgac. 1998. Function of the COOH-terminal domain of Vph1p in activity and assembly of the yeast V-ATPase. *J. Biol. Chem.* 273:6717–6723.
8. Leng, X.-H., M. F. Manolson, Q. Liu, and M. Forgac. 1996. Site-directed mutagenesis of the 100-kDa subunit (Vph1p) of the yeast vacuolar (H^+)-ATPase. *J. Biol. Chem.* 271:22487–22493.
9. Czisch, M., V. Liebers, R. Bernstein, Z. Chen, X. Baur, and T. A. Holak. 1994. Conformations of peptide fragments comprising the complete sequence of component III of Chi t and their relationship to T-Cell stimulation. *Biochemistry.* 33:9420–9427.
10. Myers, J. K., C. N. Pace, and J. M. Scholtzt. 1997. A direct comparison of helix propensity in proteins and peptides. *Proc. Natl. Acad. Sci. USA.* 94:2833–2837.
11. Lazarova, T., K. A. Brewin, K. Stoeber, and C. R. Robinson. 2004. Characterization of peptides corresponding to the seven transmembrane domains of human adenosine A_2a receptor. *Biochemistry.* 43:12945–12954.
12. Albert, A. D., and P. L. Yeagle. 2000. Domain approach to three-dimensional structure of rhodopsin using high-resolution nuclear magnetic resonance. *Methods Enzymol.* 315:107–115.
13. Wang, Y., T. Inoue, and M. Forgac. 2005. Subunit a of the yeast V-ATPase participates in binding of bafilomycin. *J. Biol. Chem.* 280: 40481–40488.
14. Duarte, A. M. S., C. J. A. M. Wolfs, N. A. J. Van Nuland, M. A. Harrison, J. B. C. Findlay, C. P. M. Van Mierlo, and M. A. Hemminga. 2006. Structure and localization of an essential transmembrane segment of the proton translocation channel of yeast H^+-V-ATPase. *Biochim. Biophys. Acta.* In press.
15. Pelton, J. T. 2001. Secondary considerations. *Science.* 16:2175–2176.
16. Rabenstein, M. D., and Y.-K. Shin. 1995. Determination of the distance between two spin labels attached to a macromolecule. *Proc. Natl. Acad. Sci. USA.* 92:8239–8243.
17. Borbat, P. P., A. J. Costa-Filho, K. A. Earle, J. K. Moscicki, and J. H. Freed. 2001. Electron spin resonance in studies of membranes and proteins. *Science.* 291:266–269.
18. Beevers, A. J., and A. Kukol. 2006. Conformational flexibility of the peptide hormone ghrelin in solution and lipid membrane bound: a molecular dynamics study. *J. Biomol. Struct. Dyn.* 23:357–363.
19. Vik, S. B., and B. J. Antonio. 1994. A mechanism of proton translocation by F_1F_0ATP synthases suggested by double mutants of the *a* subunit. *J. Biol. Chem.* 269:30364–30369.

20. Vos, W. L., L. S. Vermeer, C. J. A. M. Wolfs, R. B. Spruijt, and M. A. Hemminga. 2006. Decomposition of ESR spectra using MALDI-ToF mass spectrometry. *Anal. Chem.* 78:5296–5301.
21. Chen, Y. H., J. T. Yang, and K. H. Chau. 1974. Determination of the helix and β forms of proteins in aqueous solution by circular dichroism. *Biochemistry.* 13:3350–3359.
22. Kokorin, A. I., K. I. Zamarayev, G. L. Grigoryan, V. P. Ivanov, and E. G. Rozantsev. 1972. Measurement of the distances between the paramagnetic centres in solid solutions of nitroxide radicals, biradicals and spin-labelled proteins. *Biofizika.* 17:24–41.
23. Steinhoff, H.-J. 2002. Methods for study of protein dynamics and protein-protein interaction in protein-ubiquitination by electron paramagnetic resonance spectroscopy. *Front. Biosci.* 7:97–110.
24. Creighton, T. E. 1983. Proteins. Freeman, New York.
25. Berendsen, H. J. C., D. van der Spoel, and R. van Drunen. 1995. GROMACS: a message-passing parallel molecular dynamics implementation. *Comput. Phys. Commun.* 91:43–56.
26. Lindahl, E., B. Hess, and D. van der Spoel. 2001. GROMACS 3.0: a package for molecular simulation and trajectory analysis. *J. Mol. Mod.* 7:306–317.
27. Van Gunsteren, W. F., S. R. Billeter, A. A. Eising, P. H. Huenenberger, P. Krueger, A. E. Mark, W. R. P. Scott, and I. G. Tironi. 1996. Biomolecular Simulation: The GROMOS96 Manual and User Guide. Vdf Hochschulverlag AG an der ETH Zürich, Zürich.
28. Berendsen, H. J. C., J. P. M. Postma, W. F. Van Gunsteren, A. DiNola, and J. R. Haak. 1984. Molecular dynamics with coupling to an external bath. *J. Chem. Phys.* 81:3684–3690.
29. Tironi, I. G., R. Sperb, P. E. Smith, and W. F. Van Gunsteren. 1995. A generalized reaction field method for molecular dynamics simulations. *J. Chem. Phys.* 102:5451–5459.
30. Gargallo, R., B. Oliva, E. Querol, and F. X. Avilés. 2000. Effect of the reaction field electrostatic term on the molecular dynamics simulation of the activation domain of procarboxypeptidase B. *Protein Eng.* 13:21–26.
31. Dutta, K., A. Alex, H. Huang, and S. M. Pascal. 2001. pH-induced folding of an apoptotic coiled coil. *Protein Sci.* 10:2531–2540.
32. Zhou, N. E., C. M. Kay, and R. S. Hodges. 1994. The role of interhelical ionic interactions in controlling protein folding and stability. De novo designed synthetic two-stranded α-helical coiled-coils. *J. Mol. Biol.* 237:500–512.
33. Steinhoff, H.-J., N. Radzwill, W. Thevis, V. Lenz, D. Brandenburg, A. Antson, G. Dodson, and A. Wollmer. 1997. Determination of interspin distances between spin labels attached to insulin: comparison of paramagnetic resonance data with the x-ray structure. *Biophys. J.* 73:3287–3298.
34. Stopar, D., R. B. Spruijt, C. J. A. M. Wolfs, and M. A. Hemminga. 1997. In situ aggregational state of M13 bacteriophage major coat protein in sodium cholate and lipid bilayers. *Biochemistry.* 36:12268–12275.
35. Zagrovic, B., G. Jayachandran, I. S. Millet, S. Doniach, and V. S. Pande. 2005. How large is an α-helix? Studies of the radii of gyration of helical peptides by small-angle X-ray scattering and molecular dynamics. *J. Mol. Biol.* 353:232–241.
36. Manning, M. C., and R. W. Woody. 1991. Theoretical CD studies of polypeptide helices: examination of important electronic and geometric factors. *Biopolymers.* 31:569–586.
37. Langen, R., K. J. Oh, D. Cascio, and W. L. Hubbell. 2000. Crystal structures of spin labeled T4 lysozyme mutants: implications for the interpretation of EPR spectra in terms of structure. *Biochemistry.* 39:8396–8405.
38. Todd, A. P., and G. L. Millhauser. 1991. ESR spectra reflect local and global mobility in a short spin-labeled peptide througout the α-helix–coil transition. *Biochemistry.* 30:5515–5523.
39. Monera, O. D., N. E. Zhou, P. Lavigne, C. M. Kay, and R. S. Hodges. 1996. Formation of parallel and antiparallel coiled-coils controlled by the relative positions of alanine residues in the hydrophobic core. *J. Biol. Chem.* 271:3995–4001.
40. Lomander, A., W. Hwang, and S. Zhang. 2005. Hierarchical self-assembly of a coiled-coil peptide into fractal structure. *Nano Lett.* 5:1255–1260.
41. Galbraith, T. P., R. Harris, P. C. Driscoll, and B. A. Wallace. 2003. Solution NMR studies of antiamoebin, a membrane channel-forming polypeptide. *Biophys. J.* 84:185–194.
42. Cafiso, D. S. 1994. Alamethicin: A peptide model for voltage gating and protein-membrane interactions. *Annu. Rev. Biophys. Biomol. Struct.* 23:141–165.
43. Kabsch, W., and C. Sander. 1983. Dictionary of protein secondary structure: pattern recognition of hydrogen-bonded and geometrical features. *Biopolymers.* 22:2577–2637.
44. Weaver, T. M. 2000. The π-helix translates structure into function. *Protein Sci.* 9:201–206.
45. Fodje, M. N., and S. Al-Karadaghi. 2002. Occurence, conformational features and amino acid propensities for the π-helix. *Protein Eng.* 15:353–358.
46. Zbilut, J. P., A. Colosimo, F. Conti, M. Colafranceschi, C. Manetti, M. C. Valerio, C. L. Webber, Jr., and A. Guiliani. 2003. Protein aggregation/folding: the role of deterministic singularities of sequence hydrophobicity as determined by nonlinear signal analysis of acylphosphatase and Aβ(1–40). *Biophys. J.* 85:3544–3557.
47. Feig, M., A. D. MacKerell, and C. L. Brooks. 2003. Force field influence on the observation of π-helical protein structures in molecular dynamics simulations. *J. Phys. Chem. B.* 107:2831–2836.
48. Gilmanshin, R., S. Williams, R. H. Callender, W. H. Woodruff, and R. B. Dyer. 1997. Fast events in protein folding: relaxation dynamics of secondary and tertiary structure in native apomyoglobin. *Proc. Natl. Acad. Sci. USA.* 94:3709–3713.
49. Miick, S. M., K. M. Casteel, and G. L. Millhauser. 1993. Experimental molecular dynamics of an alanine-based helical peptide determined by spin label electron spin resonance. *Biochemistry.* 32:8014–8021.
50. Ho, B. K., A. Thomas, and R. Brasseur. 2003. Revisiting the Ramachandran plot: hard-sphere repulsion, electrostatics, and H-bonding in the α-helix. *Protein Sci.* 12:2508–2522.
51. Wang, Y., T. Inoue, and M. Forgac. 2004. TM2 but not TM4 of subunit c'' interacts with TM7 of subunit a of the yeast V-ATPase as defined by the disulfide-mediated cross-linking. *J. Biol. Chem.* 279:44628–44638.
52. Kawasaki-Nishi, S., T. Nishi, and M. Forgac. 2003. Interacting helical surfaces of the transmembrane segments of subunits a and c' of the yeast V-ATPase defined by disulfide-mediated cross-linking. *J. Biol. Chem.* 43:41908–41913.
53. Forrest, L. R., and M. S. P. Sansom. 2000. Membrane simulations: bigger and better? *Curr. Opin. Struct Biol.* 10:174–181.
54. Duneau, J.-P., S. Crouzy, Y. Chapron, and M. Genest. 1999. Dynamics of the transmembrane domain of the ErbB-2 receptor. *Theor. Chem. Acc.* 101:87–91.
55. Wegener, A. A., J. P. Klare, M. Engelhard, and H.-J. Steinhoff. 2001. Structural insights into the early steps of receptor-transducer signal transfer in archael phototaxis. *EMBO J.* 20:5312–5319.